Accepted Manuscript

Soft magnetic properties of rapidly-annealed nanocrystalline Fe-Nb-B-(Cu) alloys

R. Parsons, B. Zang, K. Onodera, H. Kishimoto, A. Kato, K. Suzuki

PII: S0925-8388(17)32207-7

DOI: 10.1016/j.jallcom.2017.06.208

Reference: JALCOM 42277

To appear in: *Journal of Alloys and Compounds*

Received Date: 7 February 2017

Revised Date: 12 June 2017

Accepted Date: 20 June 2017

Please cite this article as: R. Parsons, B. Zang, K. Onodera, H. Kishimoto, A. Kato, K. Suzuki, Soft magnetic properties of rapidly-annealed nanocrystalline Fe-Nb-B-(Cu) alloys, *Journal of Alloys and Compounds* (2017), doi: 10.1016/j.jallcom.2017.06.208.

Soft magnetic properties of rapidly-annealed nanocrystalline Fe-Nb-B-(Cu) alloys

R. Parsons[1*], B. Zang[1], K. Onodera[2], H. Kishimoto[2], A. Kato[2] and K. Suzuki[1].

[1] *Department of Materials Science and Engineering, Monash University, Clayton, VIC 3800, Australia*

[2] *Toyota Motor Corporation, Mishuku, Susono, Shizuoka 410-1193, Japan*

Abstract

Nanocrystalline Fe-*M*-B (*M* = Zr or Nb) alloys (Nanoperm) exhibit excellent soft magnetic properties when *M* content is 6 to 7 at%. Lowering the *M* content below 4 at% usually results in a coarsening of the nanocrystallites and so sets a lower limit on the *M* content for Nanoperm. In this report we have demonstrated that a highly refined, magnetically soft nanostructure can be achieved for Fe-Nb-B-(Cu) alloys with a Nb content well below 4 at% by employing a rapid annealing process which utilises a heating rate of 150 K s^{-1}. The low Nb-content of these nanocrystalline alloys brings about a high saturation magnetic polarization of 1.85 to 1.9 T, well above the upper limit of Nanoperm (1.7 T). These newly developed, bcc-Fe based nanocrystalline soft magnetic alloys which have an *M* content lower than 4 at% are named HiB-Nanoperm. HiB-Nanoperm exhibits excellent soft magnetic properties with a coercivity as low as 2.5 A m^{-1} and a high initial permeability of ~ 10^4 at 1 kHz. A possible explanation for the rapid annealing induced grain refinement observed for this Fe-*M*-B system is that the higher annealing temperatures used by this process bring about a lowering of the precursor amorphous phase viscosity which then triggers homogeneous nucleation, thereby considerably increasing the number density of bcc-Fe nucleation sites.

Keywords: rapid annealing, induced anisotropy, nanoperm, soft magnetic materials, nanocrystalline alloys, amorphous alloys

Corresponding author: Dr. Richard R. Parsons

mailto:rparsons01@gmail.com

Phone: +61 4 3166 1324

Fax: +61 3 9905 4940

1. Introduction

Electrical devices requiring magnetic flux manipulation are increasingly finding new applications in the automotive, aviation and green energy sectors. With these new applications comes a greater demand for highly energy efficient and energy dense electrical devices. These demands may be met in part through the replacement of conventional Fe-Si core materials with Fe-rich nanocrystalline soft magnetic materials, which can offer greatly reduced core losses over a wide range of applied frequencies [1–3].

Nanocrystalline soft magnetic materials, which are composed of nanoscale crystallites embedded in a residual amorphous phase, are commonly prepared from melt-spun amorphous precursors which have undergone primary crystallisation. The currently known nanocrystalline alloys can be classified based on the lattice system of their nanocrystallites [4] and are thus divided into the following families: (1) $D0_3$-Fe(Si) based alloys developed by Yoshizawa *et al*. in 1988 [1], (2) bcc-Fe based alloys developed by Suzuki *et al.* in 1990 [5] and (3) B2-$Fe_{50}Co_{50}$ based alloys developed by Willard *et al.* in 1998 [6]. These alloy systems are known as Finemet, Nanoperm and Hitperm, respectively. In addition to these well-established alloys, new bcc-Fe(Si) based nanocrystalline alloys in the Fe-Si-B-Cu and Fe-Si-P-B-Cu systems have recently been reported with enhanced saturation magnetization values up to 1.85 T [7–9].

The excellent magnetic softness of these nanocrystalline alloys is brought about by the exchange softening effect, where the effect of the local magnetocrystalline anisotropy (K_1) is suppressed by exchange interactions [10,11]. For this exchange softening effect to take place the grain size must be smaller than the natural exchange length (L_{ex}^{0} ~ 35 nm for Fe [12]) and thus, a homogeneous nanostructure with a small grain size of 10 to 20 nm is an essential requirement for good magnetic softness. Consequently, the compositional dependence of the magnetic softness in the nanocrystalline alloys often reflects the changes in the grain size. It has been reported that a high permeability of more than 10,000 can be achieved for nanocrystalline Fe-Nb-B alloys (Nanoperm), but that this high permeability is limited to a series of Nb compositions which contain a Nb content between 6 and 7 at% [2,13]. Lowering the Nb content below 4 at% is seen to result in a coarsening of the nanocrystallites and thus placed a lower practical limit on the Nb content for Nanoperm. However, it has recently been demonstrated that magnetically soft nanostructures are achievable for alloy systems which are completely free of early transition-metal additives when a rapid annealing process is employed and that a small grain size of 17 nm and a low

coercivity of 4.6 A m^{-1} are realized for a $Fe_{85}B_{13}Ni_2$ alloy [14]. This therefore suggests that by applying a rapid annealing process to a Fe-Nb-B system a highly refined nanostructure may also be achievable for alloys which contain a Nb content lower than 4 at%. This is significant as any reduction in the Nb content of Nanoperm is likely to enhance its saturation magnetic polarization. The aim of this study is therefore to investigate the effects of rapid annealing on the microstructural and magnetic properties of the Fe-Nb-B based alloys with Nb content below 4 at% and thereby clarifying if the rapid annealing process is suitable for producing Nb-poor magnetically soft nanostructures.

2. Experimental procedures

Precursor amorphous ribbons of $Fe_{100-x-y}Nb_xB_y$ (x = 0 – 4, y = 12 – 15) and $Fe_{99-x-y}Nb_xB_yCu_1$ (x = 0 – 4, y = 12 – 15) were produced by a single-roller melt spinner in an Ar atmosphere with thicknesses of ~14 to 16 µm and a width of 1 mm. The planar flow casting technique was also used for production of wide ribbons with a width of 12 mm for magnetostriction measurements. A Cu roller with a diameter of 250 mm rotating at a circumferential speed of 30 to 50 m/s was used. These as-cast ribbons were characterised by X-ray diffraction (XRD) with a Cu K_α source, transmission electron microscopy (TEM), differential thermal analysis (DTA) and thermo-magneto-gravimetric analysis (TMGA). Scherrer's formula was used for all grain size estimation except where otherwise stated. Rapid annealing was conducted in an N_2 atmosphere with samples placed inside Cu foil (~ 20 µm thickness) packets which were then clamped between two pre-heated Cu blocks for 3 to 80 s. The Cu blocks were heated by Ni-Cr resistance wire with the temperature maintained by a temperature controller and an embedded thermocouple. The heating rate is defined as the average heating rate achieved between 673 and 703 K. This temperature range was selected as it is in the region where crystallisation is expected to occur for most alloy compositions. This heating rate was estimated by placing a 1 mm diameter K-type thermocouple between the Cu blocks and monitoring by means of an oscilloscope. A maximum heating rate of 150 K s^{-1} was estimated for this experimental setup and reduced heating rates were achieved by placing different thicknesses of alumina fiber matting between the sample packet and the Cu blocks. The temperature-time profiles of each heating rate are available as supplementary data. Note that as the temperature profile during heating follows a logistic curve and that the maximum heating rate is considerably higher (> 500 K s^{-1}) at lower temperatures. Furthermore, due to the small specific surface area of the thermocouple bead with respect to the ~ 15 µm ribbons

the true heating rate experienced by these ribbons may be considerably larger. Samples were found to be cooled to near room temperature within a couple of seconds of their removal from the furnace due to their low thermal mass. Saturation magnetostriction (λ_s) was estimated using the strain gauge method as is described in more detail elsewhere [15] and density after nano-crystallisation was estimated by a He gas pycnometer. The saturation magnetic polarization ($J_s=\mu_0 M_s$) was estimated at 0.8 MA m^{-1} using a Riken BHV-35H vibrating sample magnetometer (VSM) while H_c estimations were made using a Riken BHS-40 DC hysteresis loop tracer and the relative permeability was estimated using a Hewlett Packard 4192A LF impedance analyser.

3. Results

Figure 1 shows examples of the X-ray diffraction (XRD) patterns acquired from rapidly-solidified $Fe_{100-x-y}Nb_xB_y$ ribbons in the as-cast state. All the patterns were obtained from the free side of the ribbons where the quenching rate is expected to be the lowest. Crystalline reflection peaks are absent from the patterns for the Fe-B binary alloys containing 13 and 14 at% B while a clear reflection from the (110) plane of α-Fe is evident on the pattern for $Fe_{88}B_{12}$, indicating that the minimum B content for the formation of an amorphous phase is 13 at%. Although the (110) reflection is clearly seen on the pattern for $Fe_{87}Nb_1B_{12}$, the pattern for $Fe_{86}Nb_2B_{12}$ confirms that the ribbon is mostly amorphous with only a trace of the (110) reflection. All the $Fe_{100-x-y}Nb_xB_y$ ribbons prepared in this study with $y \geq 13$ or $y = 12$ and $x > 2$ were confirmed to be fully amorphized in the as-cast state.

Fig. 2 displays thermo-magneto-gravimetric analysis (TMGA) curves acquired from these same $Fe_{100-x-y}Nb_xB_y$ alloys in the as-cast state. The TMGA signal on each curve shows a gradual decrease with temperature, reflecting the negative temperature dependence of the spontaneous magnetization. The TMGA signal diminishes at the Curie temperature (T_C) on each curve. As is well established, the addition of B increases the Curie temperature of the amorphous phase while the addition of Nb has an opposite effect [16,17].

Similar XRD and TMGA analyses were carried out for all $Fe_{100-x-y}Nb_xB_y$ ($x = 0$ to 4, $y = 12$ to 15) and $Fe_{99-x-y}Nb_xB_yCu_1$ ($x = 0$ to 4, $y = 12$ to 15) alloys and the results are summarized in Fig. 3. The original report into Fe-Nb-B-based Nanoperm [13] also investigated the glass formability of this alloy system and it was found that an as-cast single phase amorphous microstructure was only achievable for compositions with an Fe-content of less than 86 at%. In the present study the glass formability boundary for the Fe-Nb-B alloys

is seen to extend to slightly higher Fe concentrations than that described in this previous report, indicating that a greater cooling rate was achieved during casting in the present study. This suggests that with future improvements in the casting process it may become possible to produce amorphous precursors with even greater Fe-concentrations. From the contour lines in Fig. 3(a) it can be seen that for every 1 at% increase in B and Nb, T_C is shifted by approximately +25 K and -20 K respectively. From Fig. 3(b) it is clear that no changes occur to the as-cast microstructure of Fe-Nb-B with the addition of 1 at% Cu while T_C is seen to be increased by ~ 15 to 30 K by the addition of Cu, with B-poor, Nb-rich compositions showing the largest increases.

Fig. 4(a) displays DTA curves acquired from as-cast $Fe_{86-x}Nb_1B_{13}Cu_x$ (x = 0, 1) while Fig.4(b) presents XRD patterns for the same alloys in the as-cast state and after heating to 703 and 863 K at a rate of 0.67 K s^{-1}. Two exothermic peaks are evident on each DTA curve. As is well known for the Fe-Nb-B alloy system [13], the first exothermic peak of the DTA curve is identified as the primary crystallisation of the precursor amorphous phase to bcc-Fe. This is followed by a second exothermic peak which is identified as the secondary crystallization of the residual amorphous phase to Fe-B compounds, with Fe_2B and t-Fe_3B identified by XRD after annealing at 863 K.

Fig. 5(a) displays the effect of annealing temperature (T_a) on coercivity (H_c) for $Fe_{85}Nb_1B_{13}Cu_1$ which has been annealed at three different heating rates (α). With α = 1 K s^{-1}, H_c shows a dramatic increase as T_a is raised from 668 K to 678 K. These annealing temperatures correspond to the onset of primary crystallization and thus, the increase in H_c appears to be due to the formation of bcc-Fe. Although similar magnetic hardening upon primary crystallization is also seen for α = 6 K s^{-1}, the coercivity values are clearly lower than those for α = 1 K s^{-1}. Furthermore, when α = 150 K s^{-1} this magnetic hardening effect due to primary crystallization is no longer observed and the lowest coercivity (2.5 A m^{-1} at T_a = 773 K) is obtained after primary crystallization. It is clear that higher heating rates lead to considerably smaller values of H_c for $Fe_{85}Nb_1B_{13}Cu_1$, with H_c being reduced by nearly two orders of magnitude (~100 A m^{-1} to 2.5 A m^{-1}) as the heating rate is increased from 1 to 150 K s^{-1}. The temperature at which the minimum value of H_c is obtained after primary crystallisation is indicated by an arrow and, hereafter, will be referred to as the optimum annealing temperature (T_{op}) for a given composition and heating rate. The value of T_{op} is seen to be shifted systematically to higher temperatures as the heating rate is increased.

Fig. 5(b) presents the effect of α on H_c and the mean grain size (D) for $Fe_{85}Nb_1B_{13}Cu_1$ annealed at T_{op}. The results for the Cu-free $Fe_{86}Nb_1B_{13}$ alloy annealed with α = 150 K s^{-1} are also included in this figure. It is seen that the grain size of $Fe_{85}Nb_1B_{13}Cu_1$ is reduced from more than 40 nm to approximately 16 nm by an increase of heating rate from 1 to 150 K s^{-1}. A small grain size of approximately 18 nm is also obtained for the Cu-free $Fe_{86}Nb_1B_{13}$ alloy when α = 150 K s^{-1} is employed during annealing. These grain sizes are slightly larger than that reported for conventionally annealed Nanoperm (10 nm for both $Fe_{85}Nb_7B_8$ [13] and $Fe_{84}Nb_7B_9$ [18]). Still, the grain sizes are well below the natural exchange length for Fe-based alloys (L^0 ~ 35 nm) and thus, the dramatic reduction of H_c by rapid annealing is understood by taking into account the exchange softening effect [10,11]. The microstructures of these rapidly annealed $Fe_{86}Nb_1B_{13}$ and $Fe_{85}Nb_1B_{13}Cu_1$ alloys were observed by TEM. In Fig. 6, we show the bright field transmission electron micrographs and corresponding selected area diffraction patterns for rapidly annealed (α =150 K s^{-1}) (a) $Fe_{86}Nb_1B_{13}$ and (b) $Fe_{85}B_{13}Nb_1Cu_1$, with T_{op} of 783 K and 773 K respectively. Homogeneous bcc-Fe nanostructures are confirmed in these micrographs and the diffraction patterns are free of diffractions from Fe-B compounds, indicating that the metastable equilibrium between the primary bcc-Fe phase and the residual amorphous phases is maintained after the rapid annealing process.

The effects of the total annealing time on the coercivity (H_c), mean grain size (D) and saturation magnetic polarization (J_s) were investigated for rapidly annealed $Fe_{85}B_{13}Nb_1Cu_1$. Fig. 7 displays the changes in H_c, D and J_s as a function of the total annealing time for $Fe_{85}B_{13}Nb_1Cu_1$ annealed isothermally at 773 K with a heating rate of 150 K s^{-1}. Note that total annealing time includes both the time required to reach the annealing temperature and the time spent at the annealing temperature. Both the grain size and the coercivity show a tendency to increase with annealing time. Although J_s after annealing for 3 s is clearly higher than that of the as-cast state, no further change in J_s outside of the experimental error (0.01 T) is seen. It is well established that for nanocrystalline soft magnetic materials J_s is dependent upon the volume weighted average of the local saturation magnetic polarization of the crystalline (J_s^{cr}) and residual amorphous (J_s^{am}) phases such that $J_s = V_f^{cr} \cdot J_s^{cr} + (1 - V_f^{cr}) \cdot J_s^{am}$ where V_f^{cr} is the crystalline volume fraction. Since both the spontaneous magnetization and the Cure temperature of the residual amorphous phase in Nanoperm are lower than those of the bcc-Fe nanocrystallites, J_s closely reflects the volume fraction of bcc-Fe in $Fe_{85}B_{13}Nb_1Cu_1$. Therefore, as no significant change in J_s is observed with annealing

time beyond 3 s, it is considered unlikely that the variations in coercivity seen in Fig. 7 are governed by variations in V_f^{cr}. Furthermore, electron micrographs shown previously in Fig. 7(b) also confirmed the presence of a homogeneous nanocrystalline microstructure after a short 3 s annealing time and no traces of Fe-B compounds were observed by XRD for all annealing times investigated. Although it is deemed unlikely that V_f^{cr} changes with an annealing time beyond 3 s, it is important to note that the volume fraction of the residual amorphous phase in the nanostructures may be highly influential to the exchange length, and thus also to the coercivity, in two-phase nanocrystalline soft magnetic materials [19,20]. These findings suggest that the increase in H_c with annealing time is a direct result of grain coarsening, possibly through a Ostwald ripening mechanism which is known to occur after the crystallisation of metallic glasses [21]. It is therefore found that a short annealing time is preferable as this prevents grain coarsening and maintains the excellent magnetic softness which is achieved by the rapid annealing process.

Fig. 8 displays the compositional dependence of the mean grain size (D) for Fe-Nb-B and Fe-Nb-B-Cu alloys annealed at the optimum annealing temperature (T_{op}) with a heating rate of 150 K s^{-1}. Contour lines for T_{op} are also shown in these figures. It is clear from Fig. 8(a) that Nb and B both have an impact on T_{op} for rapidly annealed nanocrystalline Fe-Nb-B. It is seen that an increase in B above 13 at% results in a clear reduction of T_{op} for a given Nb content. This reflects the effect of B on the onset of the secondary crystallization reaction (T_{x2}). It has been shown that T_{x2} in Fe-B binary amorphous alloys is lowered by an increase of B content from 13 to 15 at% [22] and this was confirmed in the present study. Hence, the maximum annealing temperature which can be used without forming Fe-B compounds is lower for those Fe-B alloys which have a B content greater than 13 at%. Contrarily, Nb is known to enhance the thermal stability of the residual amorphous phase [17] and thus T_{op} tends to be higher in Nb richer compositions. The compositional dependence of grain size is relatively small in the Fe-Nb-B ternary system, with values of 18 to 20 nm seen across all Fe-Nb-B compositions. The grain size of conventionally annealed $Fe_{86-x}Nb_xB_{14}$ (x = 0, 2, 4, 5, 6 and 8) alloys has been reported [17] and it was shown that the grain size of these alloys remains as large as 50 to 70 nm for x = 0 to 4 and a small grain size below 20 nm is limited for $x \geq 5$. Thus, our results indicates that the grain size in the Fe-Nb-B alloys with Nb content lower than 4 at% is refined significantly by rapid annealing.

From Fig. 8(b) it can be seen that the addition of 1 at % Cu leads to a decrease in T_{op} at higher B concentrations for the Fe-Nb-B-Cu alloys when compared to T_{op} of the Cu-free

Fe-Nb-B alloys. Additions of Cu to Fe-based amorphous alloys are known to reduce the onset of primary crystallization and thus, the nanostructural formation process in the Fe-Nb-B-Cu alloys takes place at lower temperatures. Furthermore, T_{op} in Fe-Nb-B-Cu is now seen to be relatively insensitive to the B concentration. Unlike Fe-Nb-B, there is a large variation in D with composition, with the most Nb-rich, B-poor composition displaying grain sizes of less than 12 nm as compared to ~17 nm for B-rich Fe-B-Cu. Furthermore, D observed for Fe-Nb-B-Cu is considerably smaller overall than that of Fe-Nb-B. This grain refinement after the addition of Cu is likely a result of the well-established heterogeneous nucleation mechanism whereby Cu segregates from the amorphous phase at the early stages of annealing to form clusters which then act as nucleation sites for nanocrystallites [23]. Furthermore, this Cu clustering process is known to be enhanced by the addition of Nb, which is seen to promote a larger number density of such clusters [24]. Therefore, the reduction in grain size observed for more Nb-rich Fe-Nb-B-Cu alloys may be a direct result of this increase in nucleation sites. This is further supported by the observation that no clear grain size dependence of Nb content is observed for the Cu-free Fe-Nb-B alloys after rapid annealing.

Fig. 9 displays the compositional dependence of H_c for the Fe-Nb-B and Fe-Nb-B-Cu alloys after rapid annealing. The annealing conditions are identical to those used in Fig. 8. As with D, the variation in H_c with alloy compositions for Fe-Nb-B is relatively small, with H_c being in a range of 6 to 7 A m^{-1}, while the Cu-containing Fe-Nb-B-Cu alloy system has smaller H_c values overall. Small H_c values less than 2 A m^{-1} are obtained for the Fe-Nb-B-Cu alloys with Nb content above 2 at %. Notably, the addition of Nb is seen to have little effect on magnetic softness for the Cu-free system, but is very effective at reducing H_c for the Cu-containing system, which is in line with the variation of grain sizes shown previously. In both the Cu-containing and Cu-free alloy systems the compositions close to the glass formability limit show a larger H_c than that in the compositions with higher glass-formability. This suggests that the quenched-in crystallites in the precursor amorphous phase may hinder the magnetic softness after nano-crystallization.

Fig. 10 displays the compositional dependence of J_s for the Fe-Nb-B and Fe-Nb-B-Cu alloys after rapid annealing which were also annealed under the same conditions as those shown in Fig. 8. The addition of Nb to both the Cu-containing and Cu-free compositions is seen to greatly reduce the value of J_s due to its relatively large atomic mass, with a ~ 0.08 T reduction in J_s per 1 at% Nb. It is for this reason that J_s values in the range of 1.7 to 1.9 T can be achieved for low Nb-content (i.e., Nb of 4 at% and less) Fe-Nb-B-(Cu) alloys and that this

alloy system has been named 'HiB-Nanoperm'. Similarly, the addition of B, which has an atomic mass less than 1/8th that of Nb, results in a much smaller reduction in J_s at ~ 0.02 T per 1 at % of B. The effect that Cu has on J_s is seen to vary with composition and, as has shown for Fe-B-Cu elsewhere [25], a reduction of ~ 0.05 T is observed per 1 at% Cu for Nb-free Fe-B alloys or Fe-Nb-B alloys with 3 at % Nb. However, for intermediate Nb concentrations (*i.e.* 1 to 2 at % Nb), the reduction in J_s with the addition of Cu is less pronounced.

Fig. 11 displays the frequency dependence of relative permeability (μ_r) at 0.4 A m^{-1} for a series of rapidly-annealed Fe-Nb-B-Cu alloys with a J_s of 1.72 to 1.85 T and for a commercial Fe-based amorphous alloy (Metglas 2605-SA1) with a J_s of 1.56 T. All the rapidly-annealed nanocrystalline Fe-Nb-B-Cu alloys shown in Fig. 11 have a μ_r that is comparable to, or higher than, that of the Fe-based amorphous alloy despite having a J_s that is greater by 0.16 to 0.29 T. For $Fe_{84}Nb_2B_{13}Cu_1$ and $Fe_{84}Nb_3B_{12}Cu_1$ the μ_r remains around 10,000 at frequencies up to 10 kHz and only beings to decrease rapidly for frequencies greater than 100 kHz.

The compositional dependence of the relative permeability (μ_r) at 1 kHz has been reported for nanocrystalline Fe-Nb-B alloys annealed conventionally (i.e., with a hearing rate of less than a few K s^{-1}) [13]. A high μ_r above 5,000 was limited to Nb contents between 5 and 7 at% in these conventionally annealed alloys and their saturation magnetization is typically 1.5 to 1.6 T. However, μ_r values higher than 5,000 are obtained for $Fe_{85}Nb_1B_{13}Cu_1$, $Fe_{84}Nb_2B_{13}Cu_1$ and $Fe_{84}Nb_3B_{12}Cu_1$ alloys with J_s of 1.72 to 1.85 T when the precursor amorphous alloys are annealed rapidly with a heating rate of 150 K s^{-1}. This is readily understood by taking into account the confirmed grain refinement effect induced by rapid annealing in the Fe-Nb-B-(Cu) alloys with a Nb content below 4 at%. The high permeability above 10,000 obtained for the rapidly annealed $Fe_{84}Nb_2B_{13}Cu_1$ and $Fe_{84}Nb_3B_{12}Cu_1$ alloys clearly demonstrates that rapid annealing is an effective approach for reducing Nb content in Nanoperm and thereby enhancing their saturation magnetization.

Table 1 presents the properties of rapidly annealed Fe-Nb-B-Cu alloys along with that of conventionally annealed nanocrystalline alloys, Fe-based amorphous and conventionally crystalline Fe-Si steels. The magnetic properties of rapidly-annealed nanocrystalline $Fe_{87}B_{13}$ have also been included because of its high J_s (1.92 T), which is the highest in the $Fe_{100-x-y}Nb_xB_y$ (x = 0 – 4, y = 12 – 15) and $Fe_{99-x-y}Nb_xB_yCu_1$ (x = 0 – 4, y = 12 – 15) alloys investigated in the present study, and because this composition also exhibits a low coercivity

of less than 8 A m^{-1}. The nanocrystalline $Fe_{87}B_{13}$ alloy has a considerably larger J_s than those of other Fe-rich nanocrystalline alloys while maintaining a comparable magnetic softness. However, $Fe_{85}Nb_1B_{13}Cu_1$ is seen to still retain a relatively large J_s of 1.85 T while also demonstrating a magnetic softness equivalent to Fe-based amorphous alloys. The saturation magnetostriction (λ_s) of select rapidly annealed alloys and for Fe-based amorphous has been estimated in this study and is present in Table 1 along with values from the literature for the other alloy systems. Much like J_s, the λ_s of nanocrystalline magnetically soft magnetic materials is well established to be dependent upon the volume weight average of the local magnetostriction constants of the nanocrystalline (λ_s^{cr}) and residual amorphous (λ_s^{am}) phases such that $\lambda_s = V_f^{cr} \cdot \lambda_s^{cr} + (1 - V_f^{cr}) \cdot \lambda_s^{am}$. Based on this model, the variations of λ_s in Fe-rich nanocrystalline materials can be explained. A rough estimate of V_f^{cr} in nanocrystalline $Fe_{87}B_{13}$ may be possible through a simple mass balance. Since the Fe_3B phase forms upon decomposition of the residual amorphous phase, a chemical composition of $Fe_{75}B_{25}$ may be assumed for the residual amorphous phase and this assumption suggests a V_f^{cr} of approximately 50 %. Adopting the λ_s value of polycrystalline bcc-Fe (– 5 ppm [26]) for λ_s^{cr} and that of amorphous $Fe_{75}B_{25}$ (34 ppm [27]) for λ_s^{am}, a bulk λ_s value of 14.5 ppm is predicted for nanocrystalline $Fe_{87}B_{13}$. This is consistent with our experimental result of 14 ppm. Furthermore, the addition of Nb is known to considerably reduce λ_s^{am} [15] and so may also explain the slightly lower value of 12 ppm estimated for nanocrystalline $Fe_{85}Nb_1B_{13}Cu_1$. The volume fraction of the bcc-Fe phase in nanocrystalline $Fe_{82.5}Si_2B_{14}Cu_{1.5}$ has previously been estimated at 36 % by Mössbauer spectroscopy while λ_s^{cr} is expected to be approximately 2 ppm due to the local Si content of the crystalline phase being in the range of 3 at % [28]. From these estimations, λ_s of $Fe_{82.7}Si_2B_{14}Cu_{1.3}$ can also be predicted and is calculated to be 22 ppm, which is again in good agreement with the measured value of 21 ppm.

Importantly, rapidly annealed Fe-Nb-B-Cu alloys can also achieve a J_s comparable to that of 6.5 mass % Fe-Si steel while still maintaining a coercivity that is one tenth the size. This, in combination with an intrinsically low material thickness due to the casting process, a low material cost, good oxidation resistance and moderate glass-formability may make rapidly annealed Fe-Nb-B-(Cu) alloys attractive for commercial development. However, further investigation is still required in order to establish the frequency and field dependence of core losses, the effects of field and stress annealing and the long term thermal stability of rapidly annealed alloys. This, in addition to a more detailed investigation into the underlying

mechanism of rapid annealing induced grain refinement, will therefore be the focus of future investigations.

4. Discussion

4.1 Possible mechanism of grain refinement induced by rapid annealing

The dependence of grain size (D) on Nb content has previously been reported for $Fe_{86-x}Nb_xB_{14}$ where it was demonstrated that conventional annealing (i.e., with α less than few K s^{-1}) can only produce a highly refined nanostructure (D < 20 nm) when x ≥ 5 at % [17]. This effect was attributed to the different mechanisms of nucleation which are known to occur in amorphous metals when they are (i) well below or (ii) close to, and above, their glass transition temperature (T_g) [29]. For temperatures well below T_g the atomic transport in amorphous metals is well described by an Arrhenius-type equation [30]. However, at temperatures approaching T_g viscous flow becomes significant and so atomic transport is then best described by the Vogel-Fulcher-Tamman equation [31]. Consequently, the nucleation kinetics of amorphous metals is strongly temperature dependent in the vicinity of T_g. When nucleation occurs well below T_g it is suggested to be exclusively heterogeneous, and may occur predominantly at pre-existing nuclei [21]. However, Köster and Meinhard observed that when nucleation takes place near to, and above T_g, then the nucleation mechanism transitions to being predominantly homogeneous and that this gives rise to a greatly increased number density of nucleation sites which leads to a more refined nanostructure [30]. This same homogeneous nucleation process was suggested to occur for Fe-Nb-B based Nanoperm [29], where it was demonstrated that the addition of Nb to $Fe_{86-x}Nb_xB_{14}$ acts to enhance the thermal stability of the as-cast amorphous phase, thereby shifting the crystallisation onset temperature (T_{x1}) to higher temperatures so that when x ≥ 5 at %, $T_{x1} \geq T_g$. Hence, the transition from a coarse nanostructure to a highly refined nanostructure with increasing Nb content was seen to coincide with crystallisation taking place either well below or in the vicinity of T_g respectively.

From the present study it is clear that by combining high heating rates, high annealing temperatures and short annealing times a considerable reduction in grain size can be realised for Fe-Nb-B-(Cu) alloys. Specifically, the annealing temperature which produces a minimum coercivity (H_c) after crystallisation was shown to be significantly higher than that utilised by more conventional annealing process (again, α less than few K s^{-1}). It is therefore suggested that the elevated annealing temperatures used by the rapid annealing process may be

approaching the T_g of each respective Fe-Nb-B-(Cu) alloy and that this may bring about a high homogeneous nucleation rate. Unfortunately, T_g cannot be estimated directly for these alloy compositions due to T_{x1} being well below T_g for heating rates that can be achieved by a thermal or viscoelastic analyser. However, given the glass transition temperatures reported for amorphous $Fe_{86-x}Nb_xB_{14}$ with x = 6 and 8 (T_g = 770 to 785 K) [29], the optimum annealing temperatures employed for the rapid annealing process in the present study (753 to 883 K) are well within the vicinity of T_g. The heating rate dependence of grain size observed in this study is therefore suggested to be a result of high homogeneous nucleation rates brought about by a reduction in the viscosity of the amorphous phase at the relatively high annealing temperatures made possible by the rapid annealing process.

In this study the addition of Cu to Fe-Nb-B was also shown to reduce grain sizes even when the rapid annealing process was employed. This may suggested that a combination of both homogeneous and heterogonous nucleation may occur, with Cu-clusters acting as heterogonous nucleation sites. A recent atom-probe study by Pradeep et al. [32] reported that during the initial stages of crystallisation the number density of Cu clusters is increased by ~ 50 to 80% when rapid annealing was employed for $Fe_{73.5}Si_{15.5}Cu_1Nb_3B_7$. This suggests that the heterogeneous nucleation rate in the Fe-Nb-B-Cu alloys could also be enhanced by rapid annealing, resulting in an extra contribution to the grain refinement via the possible homogeneous nucleation process induced by rapid annealing. However, a more detailed investigation is required to clearly determine the origin of the grain refinement induced by rapid annealing in both Cu-free and Cu-containing Fe-Nb-B based nanocrystalline soft magnetic materials.

4.2 Origin of magnetic softness and high saturation magnetization in rapidly annealed Fe-Nb-B-(Cu)

Fig. 12 shows the relationship between H_c and D for the nanocrystalline $Fe_{100-x-y}Nb_xB_y$ (x = 0 to 4, y = 12 to 15) and $Fe_{99-x-y}Nb_xB_yCu_1$ (x = 0 to 4, y = 12 to 15) alloys. The largest grain sizes in this plot were obtained from the samples which were annealed at a reduced heating rate. Results from over-annealed samples containing Fe-B compounds are excluded from the plot. The coercivity follows approximately a D^3 dependence for D < 30 nm while this relationship is closer to the well-known D^6 dependence for the D range above 30 nm. It has been shown that the D^3 dependence could be observed when the exchange length (L_{ex}) is governed by induced anisotropies which are coherent over a length scale longer than L_{ex}

[11,33]. Both the D^3 and D^6 scaling behaviours have been predicted in Herzer's random anisotropy model [10,12] and the soft magnetic properties observed for the nanocrystalline Fe-Nb-B-(Cu) alloys can be explained by the exchange softening effect.

In Fig. 13(a) we show the relationship between the saturation magnetic polarization (J_s) and the total mass percentage of nonmagnetic additives for the rapidly annealed nanocrystalline Fe-Nb-B-(Cu) alloys examined in this study and also for well-known Fe-based nanocrystalline soft magnetic alloys from the literature. Alloys exhibiting poor magnetic softness with a coercivity greater than 10 A m^{-1} are excluded from this plot. It is clear that J_s is highly correlated with the mass fraction of the nonmagnetic additives. The highest J_s (1.92 T) is obtained for $Fe_{87}B_{13}$ (2.81 mass% B) simply because of its exceptionally low mass fraction of nonmagnetic additives. The addition of nonmagnetic elements with an atomic mass much larger than that of B result in J_s values lower than 1.92 T and thus, the upper limit of J_s for Si and/or P containing alloys is 1.85 T.

Fig. 13(b) shows the relationship between J_s and H_c for the rapidly annealed nanocrystalline Fe-Nb-B-(Cu) alloys from this study along with literature values [3,5,34–39] for well-known Fe-based nanocrystalline soft magnetic alloys. The lowest coercivity values, at less than 1 A m^{-1}, belong to the $D0_3$-Fe(Si) based nanocrystalline soft magnetic alloys (i.e. Finemet family), reflecting the low intrinsic magnetocrystalline anisotropy (K_1) and the low value of induced magnetic anisotropy (K_u) in the $D0_3$-Fe(Si) phase. Naturally, the saturation magnetic polarization of these $D0_3$-Fe(Si) based alloys is limited because of the massive amount of Si added for the formation of the $D0_3$ phase. The lowest coercivity for rapidly-annealed Nanoperm is 1.5 A m^{-1} and was obtained for $Fe_{83}Nb_4B_{12}Cu_1$ with a J_s of 1.64 T. This H_c value is considerably lower than the lowest H_c value reported for the bcc-Fe(Si) based nanocrystalline alloys, such as Fe-Si-B-Cu and Fe-Si-B-P-Cu, suggesting that a minor addition of Si to bcc-Fe based alloys may not be beneficial to the magnetic softness despite the fact that a large amount of Si added for the formation of $D0_3$-Fe(Si) is effective in reducing H_c. This undesirable effect of adding a small amount of Si in bcc-Fe based alloys is seen for the nanocrystalline Fe-Si-B-P-Cu alloys. Makino et al. [8] reported that the coercivity of their nanocrystalline $Fe_{84.3}Si_4B_8P_3Cu_{0.7}$ with an average grain size of 17 nm was 10 A m^{-1} while Urata et al. [37] later reported that nanocrystalline $Fe_{84.3}B_6P_9Cu_{0.7}$ with $D \approx$ 17 nm exhibited H_c = 2.9, suggesting that the bcc-Fe(Si) nanostructure becomes magnetically softer when Si is removed.

A possible reason for the undesirable effect of Si in the bcc-Fe(Si) based nanocrystalline alloys is its effect on the induced magnetic anisotropy (K_u). We have recently carried out a systematic investigation on K_u in nanocrystalline Fe-Si-B-Cu alloys and showed that the local K_u of the bcc-Fe(Si) phase was found to increase from ~50 J m^{-3} to ~170 J m^{-3} with an increase in the local Si content from 0 to 6 at% [28]. However, K_u is known to decrease when the Si content is raised beyond 6 at% such that it is approaching zero at the Fe_3Si stoichiometry [40,41]. Thus, a large induced anisotropy is expected only when a small amount of Si is added. It is worth mentioning here that the local Si content in the nanocrystallites tends to be higher than the nominal composition because Si is often partitioned preferentially to the bcc-Fe grains upon primary crystallization [28,40]. Thus, K_u in bcc-Fe(Si) based nanocrystalline alloys with Si contents of 2 to 4 at% may be considerably larger than those in the Si-free or $D0_3$-Fe(Si) based nanocrystalline alloys.

The effect of K_u in nanocrystalline soft magnetic materials has been studied elsewhere both theoretically and experimentally. It has been shown that the coercivity of nanocrystalline $Fe_{84}Nb_6B_{10}$, which has a K_u of about 100 J m^{-3}, is reduced from 10 A m^{-1} to 3 A m^{-1} by eliminating K_u through annealing under a rotating magnetic field [39]. This difference in H_c before and after the elimination of K_u is highlighted in Fig. 13(b). This reduction of H_c is well understood by taking into account the effect of K_u on the exchange correlation length (L_{ex}). At sufficiently small grain sizes the exchange averaging process reduces $\langle K_1 \rangle$ to a size where L_{ex} is instead governed by K_u and this results in the changeover from the well-known D^6 dependence to a D^3 dependence [10,11,33]. This changeover occurs when K_u is approximately twice the magnitude of $\langle K_1 \rangle$ [42]. Therefore, the exchange softening effect in bcc-Fe alloys at small grain sizes could be hindered by minor addition of Si because of the large K_u that such an addition will induce. Consequently, the combination of a high saturation magnetisation and a low coercivity in the rapidly-annealed Fe-Nb-B-(Cu) alloys (e.g. J_s = 1.85 T and H_c = 2.5 A m^{-1} for $Fe_{85}Nb_1B_{13}Cu_1$) is due to the production of a highly refined, exceptionally Fe-rich, Si-free nanostructure.

5. Conclusion

In order to clarify if the rapid annealing process is suitable for producing Nb-poor, magnetically soft nanostructure materials, the structural and magnetic properties of rapidly-solidified $Fe_{100-x-y}Nb_xB_y$ (x = 0 – 4, y = 12 – 15) and $Fe_{99-x-y}Nb_xB_yCu_1$ (x = 0 – 4, y = 12 – 15) alloys (HiB-Nanoperm) after annealing with a range of heating rate up to 150 K s^{-1} were investigated. A summary of the major results is as follows:

1. The mean grain size of Fe-Nb-B-(Cu) alloys can be reduced considerably by utilising a rapid annealing process where high heating rates are combined with relatively high annealing temperatures and short annealing times.
2. Small grain sizes of 12 to 20 nm can be achieved by utilising this rapid annealing process for the Fe-Nb-B-(Cu) alloys with a Nb content of less than 4 at%.
3. The coercivity (H_c) of rapidly annealed Fe-Nb-B-(Cu) alloys follows an approximate 3rd power dependence of the mean grain size (D) and low H_c values of 1.5 to 6 A m^{-1} are obtained along with high saturation magnetic polarization (J_s) values of 1.64 to 1.92 T. This demonstrates that rapid annealing is effective for producing magnetically soft nanostructured materials with a Nb content lower than that of Nanoperm and that this thereby enhances J_s well above the previous upper limit (1.7 T) of this alloy family.
4. The D^3 dependence implies that the magnetic softness of the rapidly-annealed Fe-Nb-B-(Cu) alloys is governed by the exchange softening effect under the influence of induced anisotropies, which are coherent over a length scale longer than the exchange correlation length.

Acknowledgments

The authors are grateful to the Australian Research Council for their financial support.

References

[1] Y Yoshizawa, S. Oguma, K. Yamauchi, New Fe based soft magnetic alloys composed of ultrafine grain structure, J. Appl. Phys. 64 (1988) 6044.
[2] K. Suzuki, A. Makino, A. Inoue, T. Masumoto, Soft magnetic properties of nanocrystalline bcc Fe□Zr□B and Fe□M□B□Cu (M= transition metal) alloys with high saturation magnetization, J. Appl. Phys. 70 (1991) 6232–6237.
[3] G. Herzer, Nanocrystalline soft magnetic alloys, in: Handb. Magn. Mater., 1997: pp. 415–462.
[4] M.E. McHenry, M.A. Willard, D.E. Laughlin, Amorphous and nanocrystalline materials for applications as soft magnets, Prog. Mater. Sci. 44 (1999) 291–433.
[5] K. Suzuki, N. Kataoka, A. Inoue, A. Makino, T. Masumoto, High Saturation Magnetization and Soft Magnetic Properties of bcc Fe-Zr-B Alloys with Ultrafine Grain Stuctures, Mater. Trans. 31 (1990) 743–746.
[6] M. Willard, D. Laughlin, M. McHenry, D. Thoma, K. Sickafus, J.O. Cross, V. Harris, Structure and magnetic properties of (FeCo) ZrBCu nanocrystalline alloys, J. Appl. Phys. 84 (1998) 6773.
[7] M. Ohta, Y. Yoshizawa, New High- B_s Fe-Based Nanocrystalline Soft Magnetic Alloys, Jpn. J. Appl. Phys. 46 (2007) L477.
[8] A. Makino, H. Men, T. Kubota, K. Yubuta, A. Inoue, New excellent soft magnetic FeSiBPCu nanocrystallized alloys with high of 1.9 T from nanohetero-amorphous phase, Magn. IEEE Trans. On. 45 (2009) 4302–4305.

[9] K. Takenaka, A.D. Setyawan, P. Sharma, N. Nishiyama, A. Makino, Industrialization of nanocrystalline Fe–Si–B–P–Cu alloys for high magnetic flux density cores, J. Magn. Magn. Mater. 401 (2016) 479–483. doi:10.1016/j.jmmm.2015.10.091.
[10] G. Herzer, Grain structure and magnetism of nanocrystalline ferromagnets, Trans. Magn. 25 (1989) 3327–3329.
[11] G. Herzer, The random anisotropy model, in: Prop. Appl. Nanocrystalline Alloys Amorph. Precursors, Springer, 2005: pp. 15–34.
[12] G. Herzer, Soft magnetic nanocrystalline materials, Scr. Metall. Mater. 33 (1995) 1741–1756.
[13] K. Suzuki, A. Makino, A. Inoue, T. Masumoto, Formation of nanocrystalline structures by crystallization of amorphous Fe-MB (M= IVa to VIa group metal) alloys, 39 (1994) 133–140 [NAID: 110004640480], see http://ci.nii.ac.jp/naid/110004640480/en/.
[14] K. Suzuki, R. Parsons, B. Zang, K. Onodera, H. Kishimoto, A. Kato, Copper-free nanocrystalline soft magnetic materials with high saturation magnetization comparable to that of Si steel, Appl. Phys. Lett. 110 (2017) 12407.
[15] R. Parsons, T. Yanai, H. Kishimoto, A. Kato, M. Ohnuma, K. Suzuki, Induced magnetic anisotropy in Si-free nanocrystalline soft magnetic materials: A transmission x-ray diffraction study, J. Appl. Phys. 117 (2015) 17A333.
[16] C. Graham, T. Egami, Magnetic properties of amorphous ribbon, Magn. IEEE Trans. On. 15 (1979) 1398–1403. doi:10.1109/TMAG.1979.1060428.
[17] K. Suzuki, J. Cadogan, V. Sahajwalla, A. Inoue, T. Masumoto, The role of alloying elements in Cu-free nanocrystalline Fe-Nb-B soft magnetic alloys, Mater. Sci. Eng. A. 226 (1997) 554–558.
[18] K. Suzuki, A. Makino, A. Inoue, T. Masumoto, Low core losses of nanocrystalline Fe–M–B (M= Zr, Hf, or Nb) alloys, J. Appl. Phys. 74 (1993) 3316–3322.
[19] K. Suzuki, J. Cadogan, Random magnetocrystalline anisotropy in two-phase nanocrystalline systems, Phys. Rev. B. 58 (1998) 2730.
[20] K. Suzuki, J. Cadogan, The effect of the spontaneous magnetization in the grain boundary region on the magnetic softness of nanocrystalline materials, J. Appl. Phys. 85 (1999) 4400–4402.
[21] U. Köster, U. Herold, Crystallization of metallic glasses, in: Glas. Met. I, Springer, 1981: pp. 225–259.
[22] M. Takahashi, M. Koshimura, T. Abuzuka, Phase diagram of amorphous and crystallized Fe-B alloy system, Jpn. J. Appl. Phys. 20 (1981) 1821.
[23] K. Hono, K. Hiraga, Q. Wang, A. Inoue, T. Sakurai, The microstructure evolution of a $Fe_{73.5}Si_{13.5}B_9Nb_3Cu_1$ nanocrystalline soft magnetic material, Acta Metall. Mater. 40 (1992) 2137–2147.
[24] J. Ayers, V. Harris, J. Sprague, W. Elam, On the role of Cu and Nb in the formation of nanocrystals in amorphous Fe73. 5Nb3Cu1Si13. 5B9, Appl. Phys. Lett. 64 (1994) 974–976.
[25] B. Zang, R. Parsons, K. Onodera, H. Kishimoto, A. Kato, A. Liu, K. Suzuki, Effect of heating rate during primary crystallization on soft magnetic properties of melt-spun Fe-B alloys, Scr. Mater. 132 (2017) 68–72.
[26] T. Yamamoto, The Developments of Sendust and Other Ferromagnetic Alloys, Comm. Acad. Achiev. (1980) 320.
[27] R.C. O'Handley, M.C. Narasimhan, M.O. Sullivan, Magnetostriction of $Fe_{100-x}B_x$ glasses, J. Appl. Phys. 50 (1979) 1633–1635. doi:http://dx.doi.org/10.1063/1.327273.
[28] R. Parsons, J. Garitaonandia, T. Yanai, K. Onodera, H. Kishimoto, A. Kato, K. Suzuki, Effect of Si on the field-induced anisotropy in Fe-rich nanocrystalline soft magnetic alloys, J. Alloys Compd. 695 (2017) 3156–3162.
[29] K. Suzuki, J. Cadogan, K. Aoki, A. Tsai, A. Inoue, T. Masumoto, Nanocrystallization and glass transition in Cu-Free Fe-Nb-B soft magnetic alloys, Scr. Mater. 44 (2001) 1417–1420.
[30] U. Köster, J. Meinhardt, Crystallization of highly undercooled metallic melts and metallic glasses around the glass transition temperature, Mater. Sci. Eng. A. 178 (1994) 271–278.
[31] D.R. Uhlmann, Crystallization and glass formation, J. Non-Cryst. Solids. 73 (1985) 585–592.

[32] K. Pradeep, G. Herzer, P. Choi, D. Raabe, Atom probe tomography study of ultrahigh nanocrystallization rates in FeSiNbBCu soft magnetic amorphous alloys on rapid annealing, Acta Mater. 68 (2014) 295–309.
[33] K. Suzuki, G. Herzer, J.M. Cadogan, The effect of coherent uniaxial anisotropies on the grain-size dependence of coercivity in nanocrystalline soft magnetic alloys, J. Magn. Magn. Mater. 177–181 (1998) 949–950.
[34] M. Ohta, Y. Yoshizawa, Magnetic properties of nanocrystalline FeCuSiB alloys, Appl. Phys. Lett. 91 (2007) 62517.
[35] N. Ito, K. Suzuki, J.S. Garitaonandia, J.D. Cashion, Effect of boron on the field-induced magnetic anisotropy in Fe-based soft magnetic nanostructures, J. Appl. Phys. 105 (2009) 07A321.
[36] A. Makino, Nanocrystalline Soft Magnetic Fe-Si-B-P-Cu Alloys With High B of 1.8–1.9T Contributable to Energy Saving, IEEE Trans. Magn. 48 (2012) 1331–1335. doi:10.1109/TMAG.2011.2175210.
[37] A. Urata, M. Yamaki, K. Satake, H. Matsumoto, A. Makino, Magnetic properties and structure of Fe83.3–85.8B7.0–4.5P9Cu0. 7 nanocrystalline alloys, J. Appl. Phys. 113 (2013) 17A311.
[38] S. Jafari, A. Beitollahi, B.E. Yekta, T. Ohkubo, V. Budinsky, M. Marsilius, G. Herzer, K. Hono, Atom probe analysis and magnetic properties of nanocrystalline $Fe_{84.3}Si_4B_8P_3Cu_{0.7}$, J. Alloys Compd. 674 (2016) 136–144. doi:10.1016/j.jallcom.2016.03.005.
[39] N. Ito, J. Michels, J. Kohlbrecher, J. Garitaonandia, K. Suzuki, J.D. Cashion, Effect of magnetic field annealing on the soft magnetic properties of nanocrystalline materials, J. Magn. Magn. Mater. 316 (2007) 458–461.
[40] G. Herzer, Nanocrystalline soft magnetic materials, Phys. Scr. 1993 (1993) 307.
[41] G. Herzer, Magnetic field-induced anisotropy in nanocrystalline Fe-Cu-Nb-Si-B alloys, J. Magn. Magn. Mater. 133 (1994) 248–250.
[42] K. Suzuki, N. Ito, J. Garitaonandia, J. Cashion, G. Herzer, Local random magnetocrystalline and macroscopic induced anisotropies in magnetic nanostructures, J. Non-Cryst. Solids. 354 (2008) 5089–5092.
[43] S. Jafari, A. Beitollahi, B. Eftekhari Yekta, T. Ohkubo, V. Budinsky, M. Marsilius, S. Mollazadeh, G. Herzer, K. Hono, Three-dimensional atom probe analysis and magnetic properties of $Fe_{85}Cu_1Si_2B_8P_4$ melt spun ribbons, J. Magn. Magn. Mater. 401 (2016) 1123–1129. doi:10.1016/j.jmmm.2015.10.106.
[44] M. Ohta, Y. Yoshizawa, Effect of Heating Rate on Soft Magnetic Properties in Nanocrystalline $Fe_{80.5}Cu_{1.5}Si_4B_{14}$ and $Fe_{82}Cu_1Nb_1Si_4B_{12}$ Alloys, Appl. Phys. Express. 2 (2009) 23005.
[45] JFE Steel Corporation Electric Steel Catalogue, (2016).
[46] C.-W. Chen, Magnetism and metallurgy of soft magnetic materials, Courier Corporation, 2013.

Table 1. A summary of the coercivity (H_c), saturation magnetic polarization (J_s), saturation magnetostriction (λ_s) and density (ρ) of nanocrystalline, amorphous and conventionally crystalline materials.

Alloys	H_c ($A \cdot m^{-1}$)	J_s (T)	λ_s (ppm)	ρ ($g \cdot cm^{-3}$)
$Fe_{83}Nb_4B_{12}Cu_1$	1.5	1.64	-	7.69
$Fe_{84}Nb_3B_{12}Cu_1$	2.0	1.72	-	7.68
$Fe_{84}Nb_2B_{13}Cu_1$	2.1	1.75	-	7.65
$Fe_{85}Nb_1B_{13}Cu_1$	2.5	1.85	12[#]	7.64
$Fe_{87}B_{13}$	6.0	1.92	14[#]	7.62
$Fe_{82.7}Si_2B_{14}Cu_{1.3}$ [7]	6.5	1.85	21[#]	-
$Fe_{85}Si_2B_8P_4Cu_1$ [36,43]	5.8	1.82	2.3 to 13.5	-
Fe-based amorphous (Metglas 2605SA1)	2.4	1.56	41[#]	7.20
Fe-based amorphous (HB1 Alloy) [44]	1.5	1.64	-	-
Non-oriented Fe-3.0%Si [45,46]	55	2.05	7.8[^]	7.64-7.76
Non-oriented Fe-6.5%Si [45]	18.5	1.80	0.1[^]	7.49

[#] Saturation magnetostriction estimated in this study by strain gauge method.

[^] Saturation magnetostriction at 1 T, 400 Hz (Sine wave).

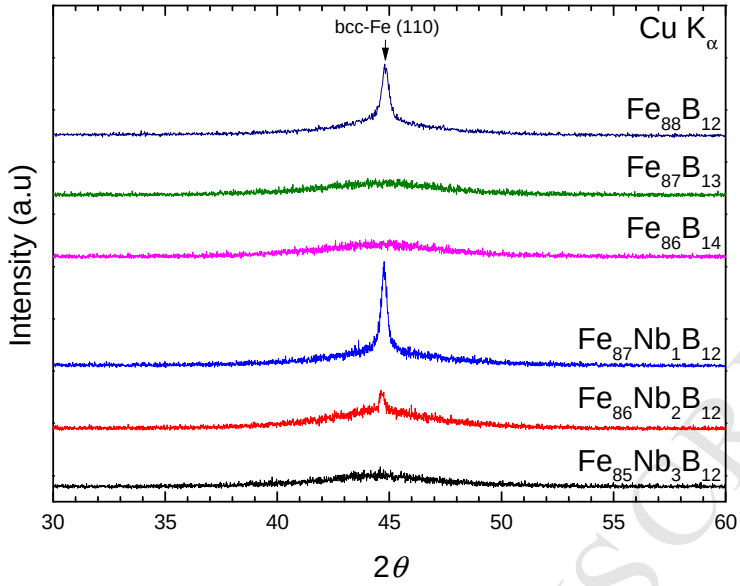

Figure 1. X-ray diffraction (XRD) patterns acquired from as-cast $Fe_{100-x-y}Nb_xB_y$ (x = 0 to 3 and y = 12 to 14).

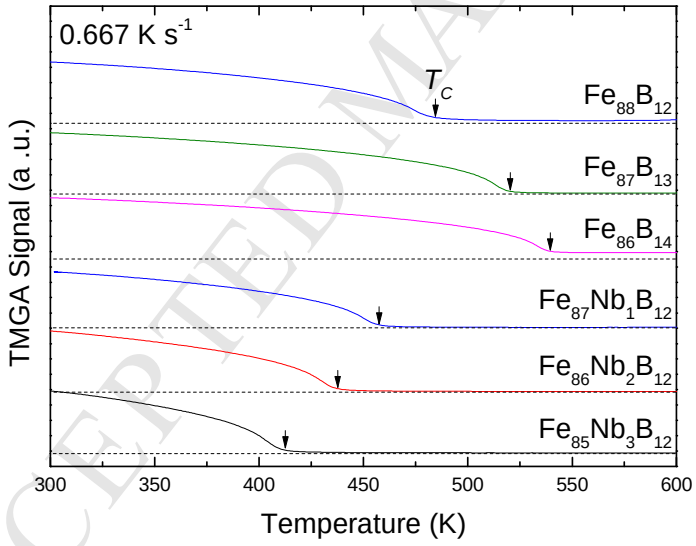

Figure 2. Thermo-magneto-gravimetric analysis (TMGA) curves acquired from as-cast $Fe_{100-x-y}Nb_xB_y$ (x = 0 to 3 and y = 12 to 14).

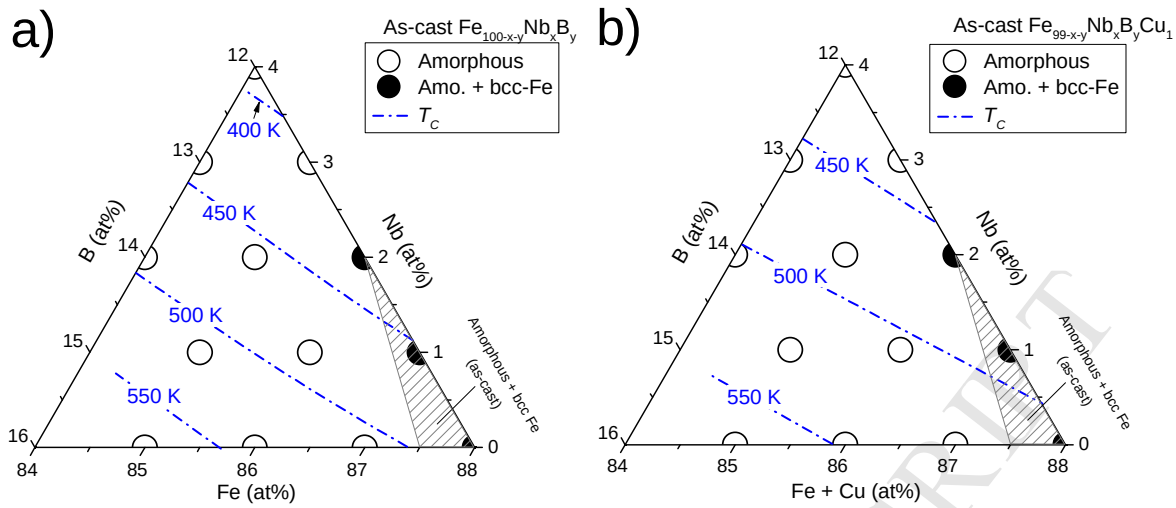

Figure 3. The phases identified by X-ray diffraction and the amorphous phase Curie temprature (T_C) contour lines for as-cast (a) $Fe_{100-x-y}Nb_xB_y$ (x = 0 – 4, y = 12 – 15) and (b) $Fe_{99-x-y}Nb_xB_yCu_1$ (x = 0 – 4, y = 12 – 15).

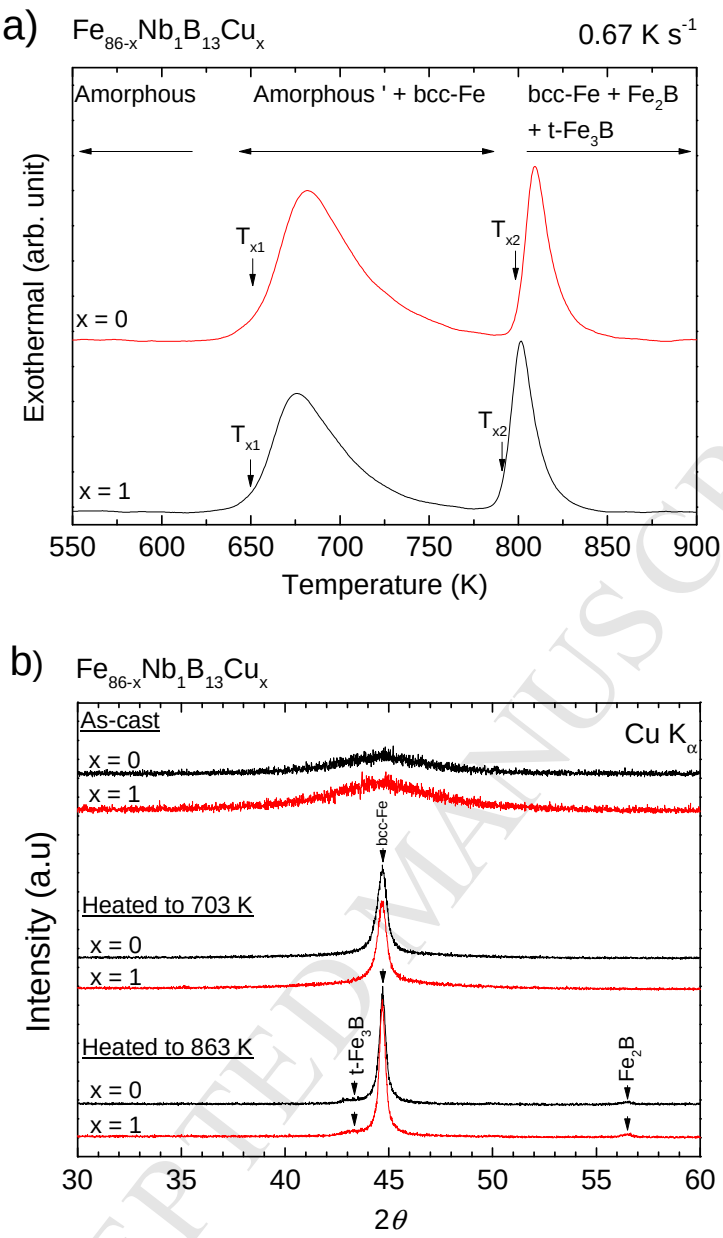

Figure 4. (a) Differential thermal analysis (DTA) curves acquired from as-cast ribbons and (b) X-ray diffraction (XRD) patterns acquired $Fe_{86-x}Nb_1B_{13}Cu_x$ (x = 0, 1) in the as-cast state and after heating (0.67 K s^{-1}) to 703 and 863 K.

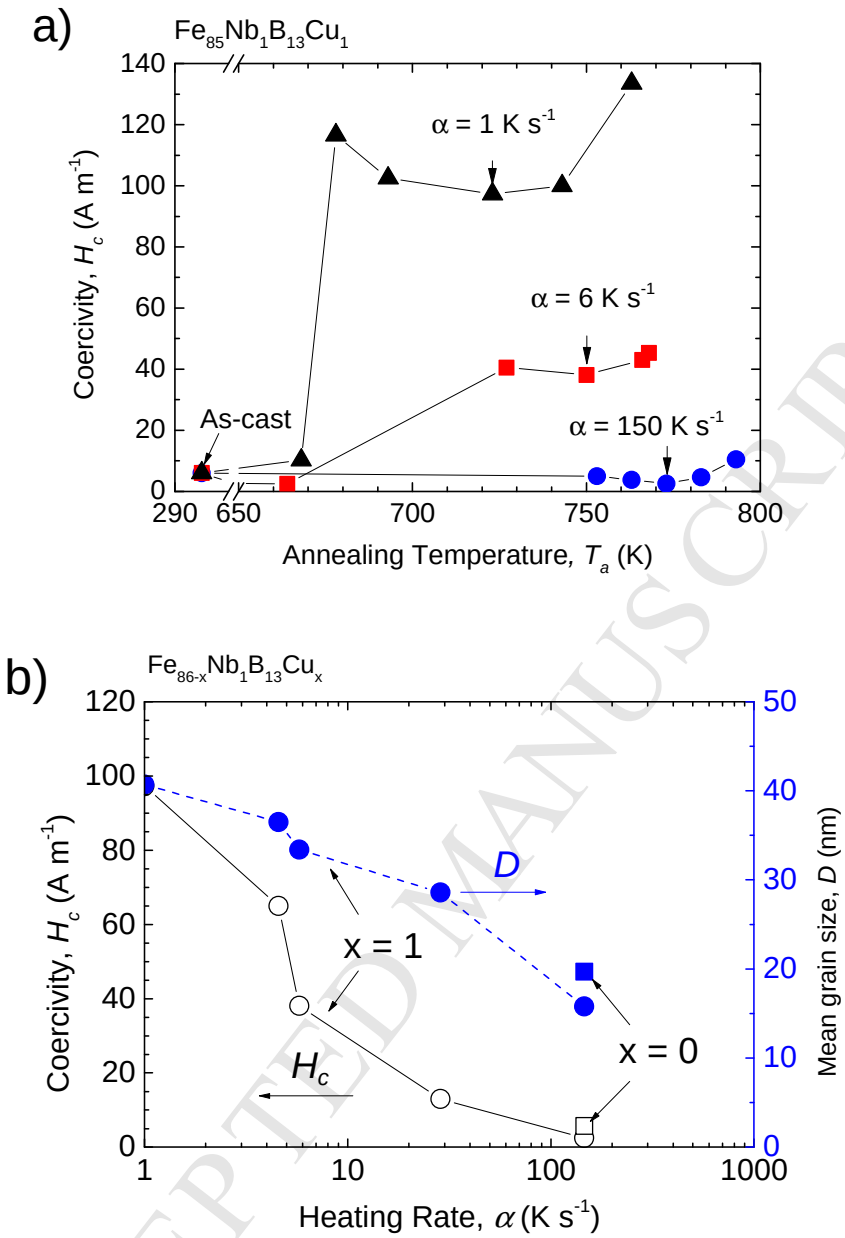

Figure 5. (a) Effect of annealing temperature (T_a) on coercivity (H_c) for $Fe_{85}Nb_1B_{13}Cu_1$ annealed with different heating rates (α) and (b) effect of α on H_c and mean grain size (D) for $Fe_{86-x}Nb_1B_{13}Cu_x$ (x = 0, 1). Note that for α < 6 K s^{-1} a conventional IR furnace was utilised.

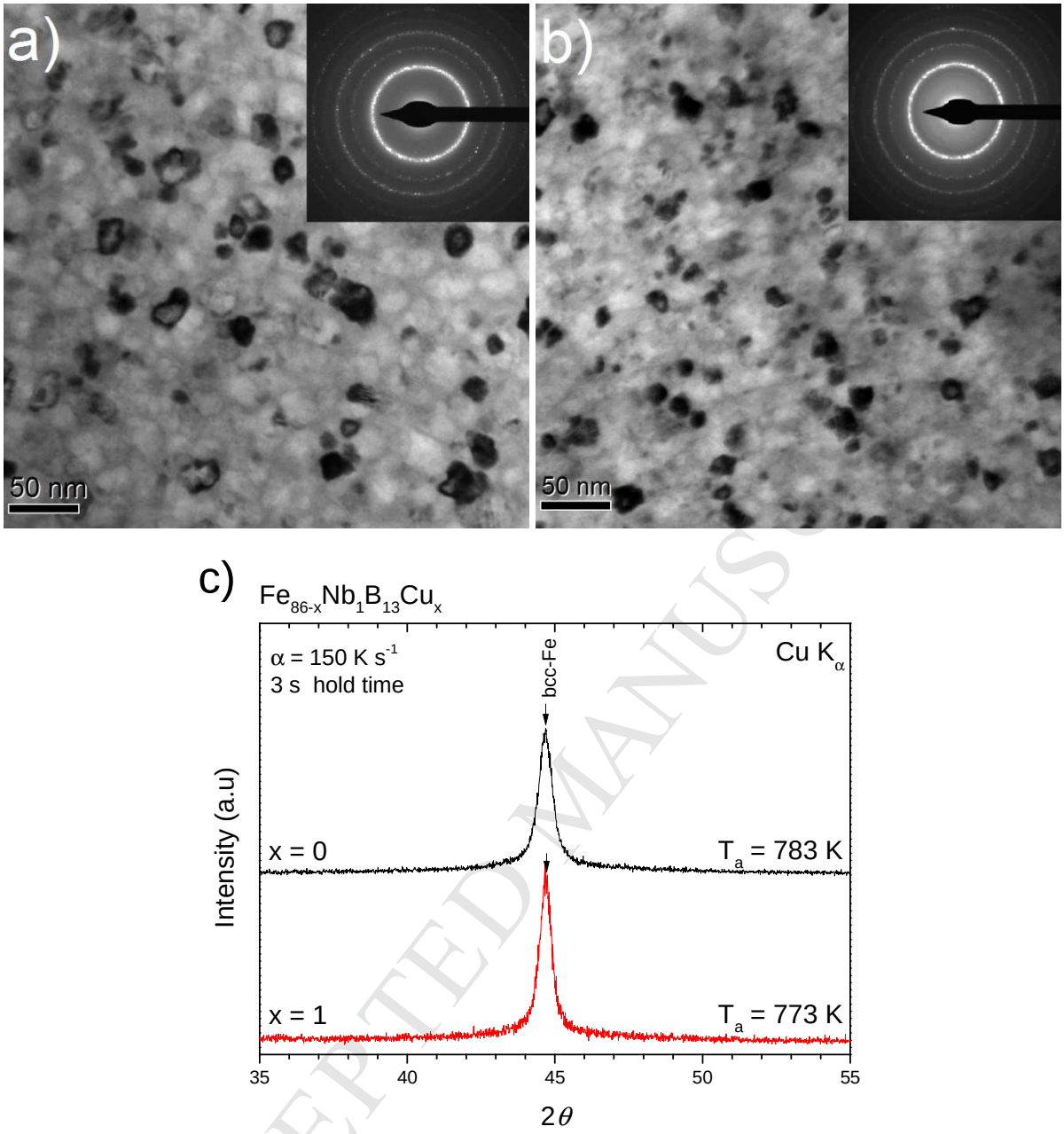

Figure 6. Bright field transmission electron microscopy (TEM) and selected area diffraction patterns for rapidly annealed (heating rate of 150 K s^{-1}) $Fe_{86}Nb_1B_{13}$ annealed at 783 K (a) and $Fe_{85}Nb_1B_{13}Cu_1$ annealed at 773 K (b) along with the corresponding x-ray diffraction patterns (c).

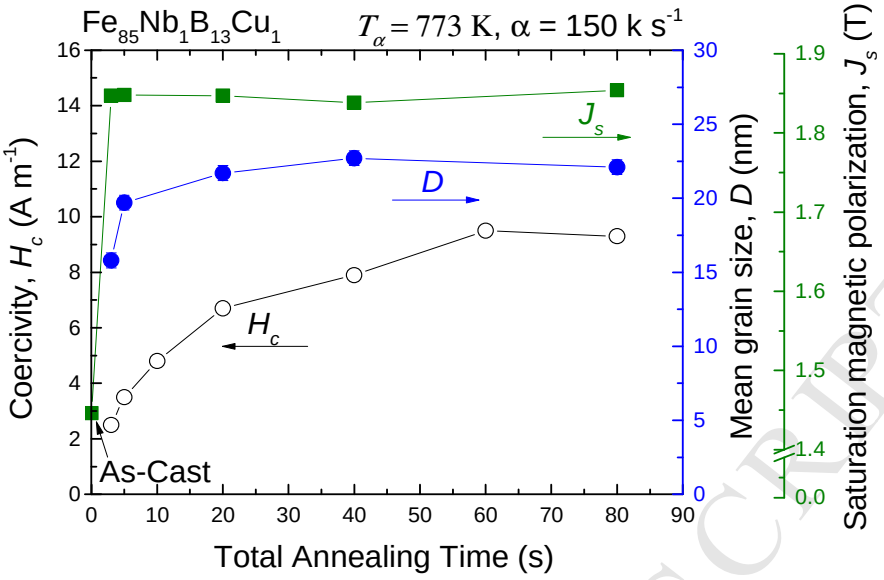

Figure 7. Effect of the total annealing time on coercivity (H_c), mean grain size (D) and saturation magnetic polarization (J_s) for $Fe_{85}Nb_1B_{13}Cu_1$ annealed at a temperature (T_a) of 773 K with a heating rate (α) of 150 K s^{-1}. Note that the total annealing time includes the time required for the sample to reach the annealing temperature, which was estimated to take no more than 3 s, and the time spent at the annealing temperature T_a.

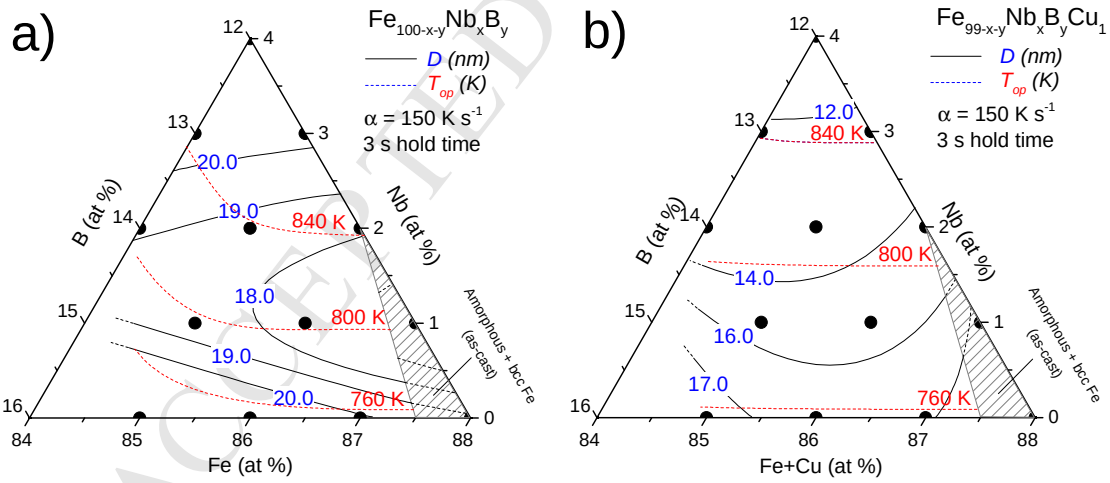

Figure 8. Ternary mapping of the mean grain size (D) and optimal annealing temperature (T_{op}) when rapidly annealing with a heating rate (α) of 150 K s^{-1} for (a) $Fe_{100-x-y}Nb_xB_y$ (x = 0 – 4, y = 12 – 15) and (b) $Fe_{99-x-y}Nb_xB_yCu_1$ (x = 0 – 4, y = 12 – 15).

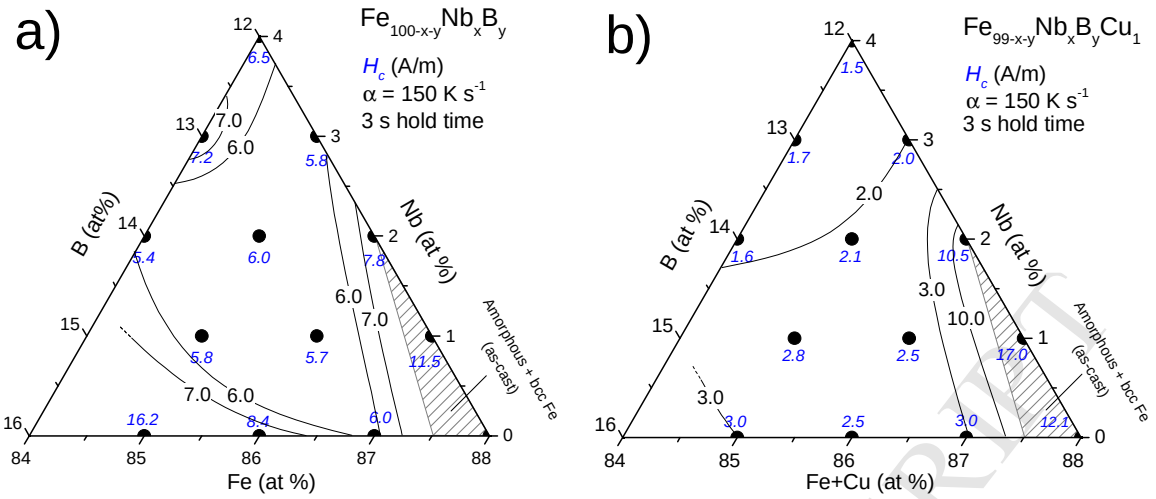

Figure 9. Ternary mapping of coercivity (H_c) for (a) $Fe_{100-x-y}Nb_xB_y$ (x = 0 – 4, y = 12 – 15) and (b) $Fe_{99-x-y}Nb_xB_yCu_1$ (x = 0 – 4, y = 12 – 15).

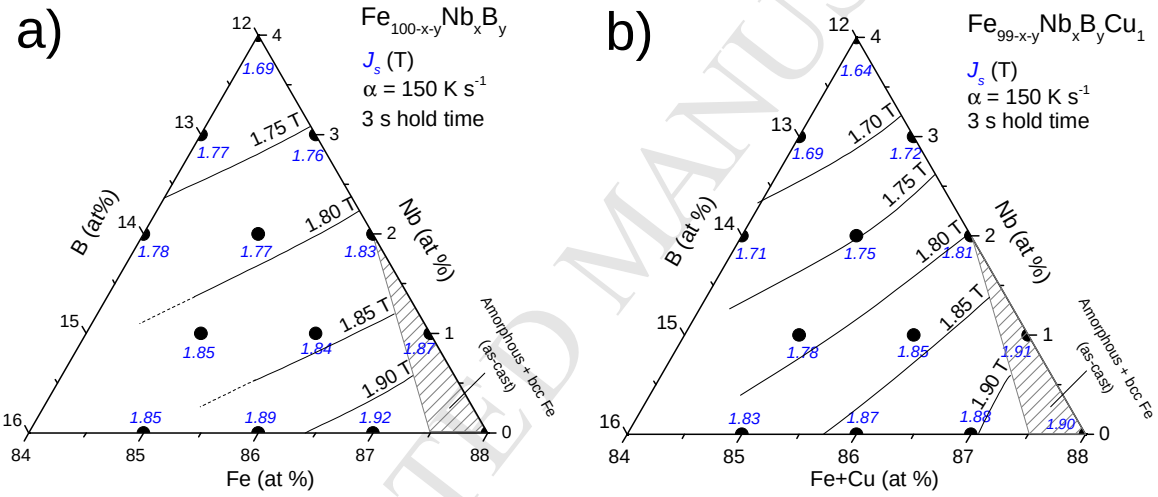

Figure 10. Ternary mapping of the saturation magnetic polarization (J_s) for (a) $Fe_{100-x-y}Nb_xB_y$ (x = 0 – 4, y = 12 – 15) and (b) $Fe_{99-x-y}Nb_xB_yCu_1$ (x = 0 – 4, y = 12 – 15). J_s uncertainty estimated to be 0.01 T.

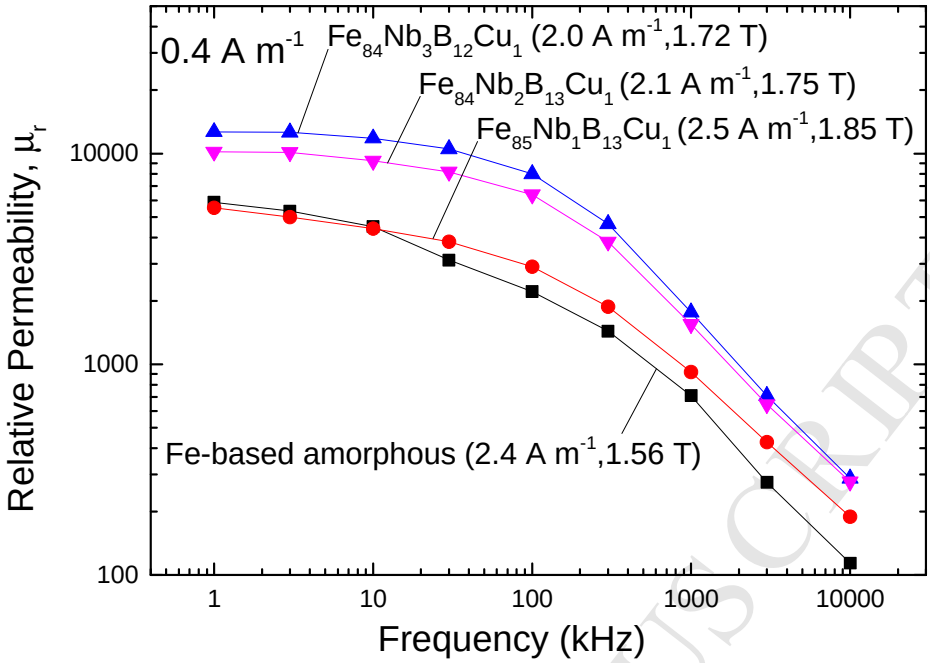

Figure 11. The dependence of relative permeability (μ_r) on frequency at 0.4 A m^{-1} for a series of nanocrystalline rapidly annealed Fe-Nb-B-Cu alloys and for a comercially produced Fe-based amorphous alloy.

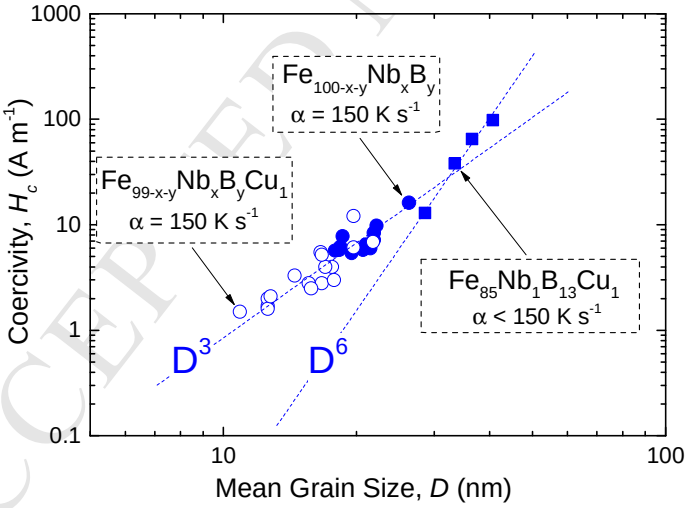

Figure 12. Coercivity (H_c) with respect to the mean grain size (D) for $Fe_{100-x-y}Nb_xB_y$ (x = 0 – 4, y = 12 – 15) and $Fe_{99-x-y}Nb_xB_yCu_1$ (x = 0 – 4, y = 12 – 15). Samples were annealed with a maximum heating rate of 150 K s^{-1} (circles) and with a reduced heating rates (squares).

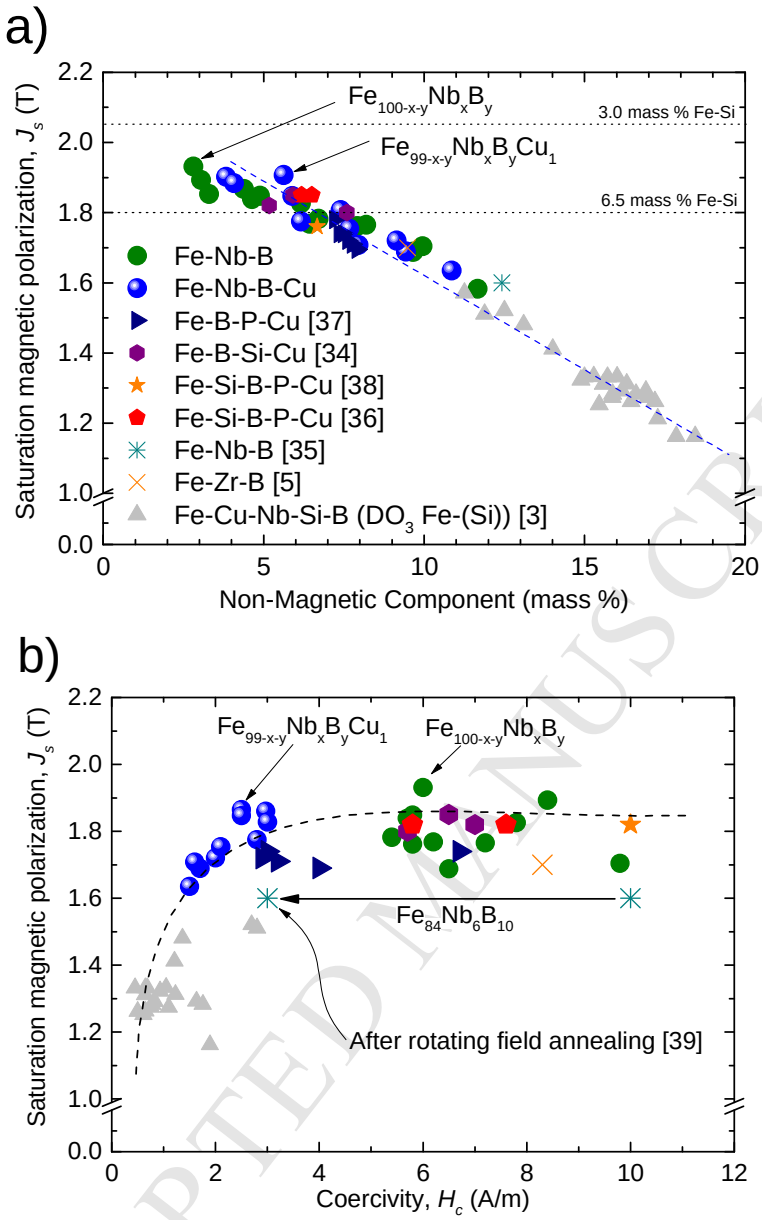

Figure 13. (a) Saturation magnetic polarization (J_s) with respect non-magnetic mass percentage and (b) with coercivity (H_c) for Fe-rich nanocrystalline magnetically soft materials. Rapidly annealed Fe-Nb-B (green circles) and Fe-Nb-B-Cu (blue spheres) are shown alongside literature values [3,5,34–39].

Highlights:

- Effect of rapid annealing studied for Fe-Nb-B-(Cu) nanocrystalline alloys.
- Small grain sizes of 12 to 20 nm can be achieved by rapid annealing process.
- Low H_c of 1.5 to 6 A m^{-1} and high J_s of 1.64 to 1.92 T obtained by rapid annealing.
- Short, high temperature, high heating rate annealing gives most grain refinement.
- Magnetic softness after rapid annealing may be governed by induced anisotropies.